Design and Implementation of Optical Wireless Communications with Optically Powered Smart Dust Motes

Dominic C. O'Brien, *Member, IEEE*, Jing Jing Liu , *Student Member, IEEE*, Grahame E. Faulkner, Sashigaran Sivathasan, *Member, IEEE*, Wei Wen Yuan, Steve Collins *Member, IEEE*, and Steve J. Elston

***Abstract*—Complete electronic and micro-mechanical systems can now be fabricated on the scale of hundreds of microns. Implementing radio frequency wireless communications with such 'smart dust' is challenging, due to the power required and the small size of any antennas that can be implemented. Optical wireless communications, using a modulated retro-reflector at the smart dust has the advantages of low-power consumption and highly directive channels that allow long communications ranges. In this paper we report the design and implementation of a communications system that uses a base station to communicate with, and power, smart dust motes, over ranges of 10s of metres. A base station that uses holographic beamsteering is described, and dust motes that use silicon ICs to provide communications, power and modulation control. Results indicate the dust mote will operate at a range of over 30m from the base station.**

***Index Terms*—Optical Wireless Communications, Smart Dust, Optically powered.**

I. Introduction

THE CONTINUAL reduction in the size of features used in Integrated Circuits (ICs) means that highly complex systems (micro-machines or smart dust) can be fabricated in very small volumes [1], [2], [3], [4], [5], [6]. Providing connections with these systems is becoming increasingly challenging [7] . Integrated circuits without wired connections are therefore attractive, and these require wireless power and communications. For structures on scale of 100s of microns and below it is difficult to create efficient RF wireless communications, as the antenna size is small compared with typical wavelengths, leading to low directivity. Optical wireless communications is an attractive alternative, as the wavelength is much smaller than the micro-machine, allowing small directive structures to be fabricated. In addition a beam of light that illuminates the machine can be used to provide power, albeit at low levels. Providing communications from these small devices to an external node is challenging. For conventional optical communications a source is required, together with a means to direct it (see work reported in [1]). These may be appropriate where high speed operation is desirable, but for low data rate communications modulated retro-reflectors are an attractive option[4], [8]. In these systems the illuminating beam is retro-reflected back to the source, and a modulator alters the intensity of the beam, thus allowing a data signal to be superimposed onto it. This allows low speed communications without the need for the smart-dust to perform tracking, and to contain an optical source. In this paper we describe the design and fabrication of a system that uses retro-reflecting channels to communicate with a smart dust mote fabricated from a CMOS integrated circuit. Section II gives an overview of the system, and the basic design constraints. In section III the design of the base station is described. Section IV describes the motes, section V describes system results and Section VI draws some conclusions.

Manuscript received 15 January 2009; revised 11 May 2009. This work was supported by the UK Engineering and Physical Sciences Research Council (EPSRC).

When this work was done all the authors were with the Department of Engineering Science, Parks Road, Oxford, OX1 3PJ, UK (e-mail: dominic.obrien@eng.ox.ac.uk).

SS is now with the School of Engineering and Science, Curtin University of Technology, CDT 250, Sarawak, 98009 Miri, Malaysia.

Digital Object Identifier 10.1109/JSAC.2009.091214.

II. Overview

Figure 1 shows a schematic of the system. A Base Station (BS) is situated above a number of Smart Dust Motes (SDMs), at a design range of up to 30m in the system considered. Light from the BS is directed toward a particular mote using a holographic beamsteering system. The light illuminates the SDM, providing power, and is also modulated to provide a downlink from the BS to the SDM. A Modulated Retro-Reflector (MRR) on the SDM reflects light back to the BS, and uses a Liquid Crystal (LC) shutter to modulate the returned beam. This modulated radiation is detected using an imaging receiver that consists of a high frame-rate CMOS camera and associated image processing. MRRs have been implemented using semiconductor based shutters[9], direct modulation of MEMs corner cube structures[10], as well as LCs. The energy consumption of different types of MRR is related to CV^2 where C is their capacitance and V is the voltage that must be applied to change the overall reflection from the device sufficiently to transmit one bit. Typical energies for MEMs based devices are 40 $\mathrm{pJ/bit}$ for a 0.5x0.5mm retro-reflector[10]. Semiconductor based Multi-Quantum Well (MQW) modulators have capacitances of approximately 50 $\mathrm{pF/mm^2}$ [11] and for a 0.5x0.5mm device would have a switching energy of (assuming a 5V switching voltage) of 300pJ. LCs have lower capacitance and switching voltage than the alternatives and are relatively straightforward to fabricate, so for the low speed application considered here are an attractive choice.

III. Base Station Design

The base station must illuminate the SDMs to provide power, sufficient intensity for the SDM downlink receiver, and

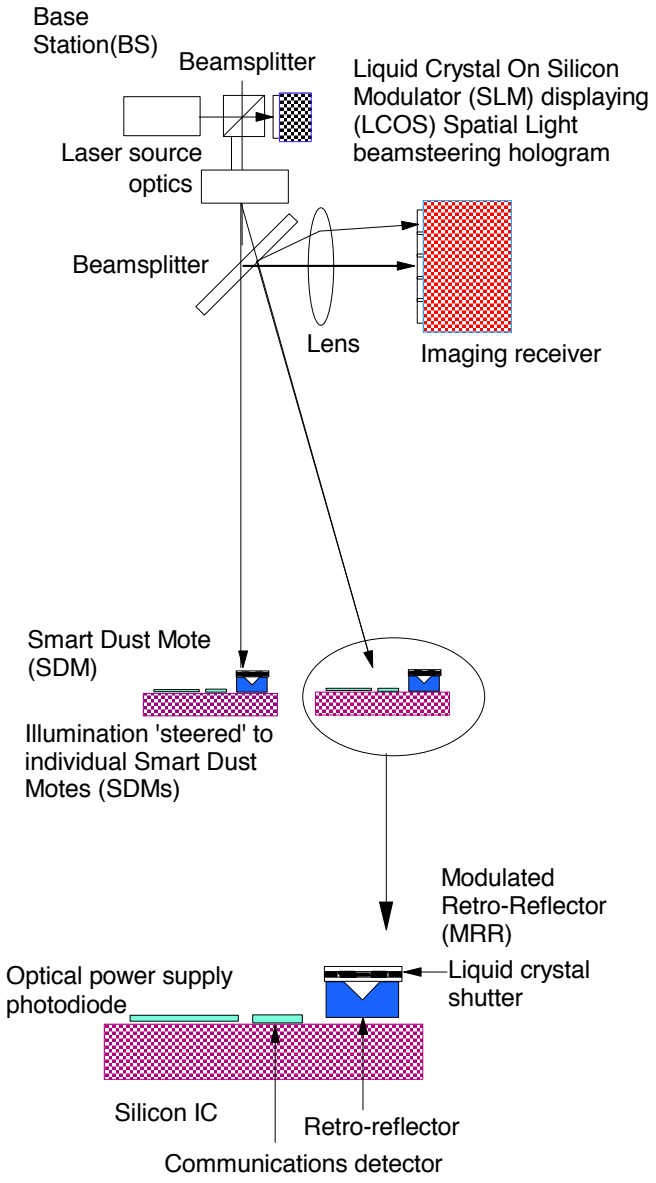

Fig. 1. Micromachine communications network

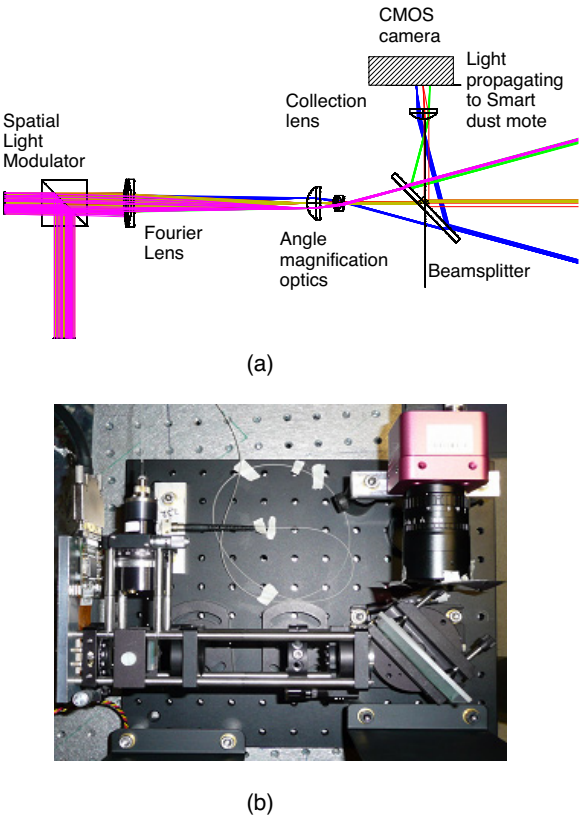

Fig. 2. (a) Optical system layout (b) Base station

sufficient power for the uplink to operate. In order to maximise the intensity at the motes a holographic beamsteering approach is used to direct a narrow beam of light to each SDM. This uses a ferroelectric liquid crystal (FLC) silicon backplane spatial light modulator (LCOS SLM) device[12]. Binary phase elements can be written to the device, and these can be used for beamsteering to multiple locations simultaneously[13]. In addition it is possible to alter the divergence of beams, and correct for aberrations in the optical system. This will be used in the acquisition and tracking phase described in later sections.

A. Optical design and link budget modeling

Figure 2(a) shows a layout of the optical system and (b) shows a picture of the completed BS. Light from a 670nm laser is polarized and illuminates the SLM. The SLM is arranged for binary phase modulation, and resulting wavefront is Fourier transformed using a Fourier Lens. The SLM can diffract light through a range of angles in x and y directions given (using a small angle approximation) by $\frac{\lambda}{\Delta} \times \frac{\lambda}{\Delta}$ where is the wavelength of operation and is the pitch of the SLM. This is 12.8 μm, so the routing angle available is 3x3 degrees. Two lenses are used to magnify the steering angle, to create a total field of view of 30 degrees (full-angle). The simple optical system used creates aberrated, enlarged, spots, which can be (approximately) corrected by adding focusing power to the beamsteering hologram, depending on the steering angle and range.

B. Intensity and link budgets

There are three constraints on the correct operation of the SDM and communications links. There must be (i) sufficient illumination intensity from the interrogating beam to power the SDM, (ii) sufficient link margin for the downlink and (iii) sufficient link margin for the uplink. Initial modelling used an analytical approach based on that used in [14] in order to obtain an approximate on-axis range of operation, then a more detailed ray-tracing simulation was used for on- and off-axis SDM positions. The parameters used for the initial simulation are shown in Table I. It is assumed that a Lambertian beam with an order m is launched from the BS. The order m is set so that the half-angle matches the diffraction limited divergence caused by the SLM aperture. Light propagates to the SDM, where it illuminates a retro-reflector, whose aperture is defined by a circular LC modulator on top of it. The intensity at the SDM can be estimated as;

$$I = \frac{(m+1)P_T}{2\pi r^2} \tag{1}$$

where m is the order of the Lambertian source, P_T is the transmitted power (measured at the output aperture of the

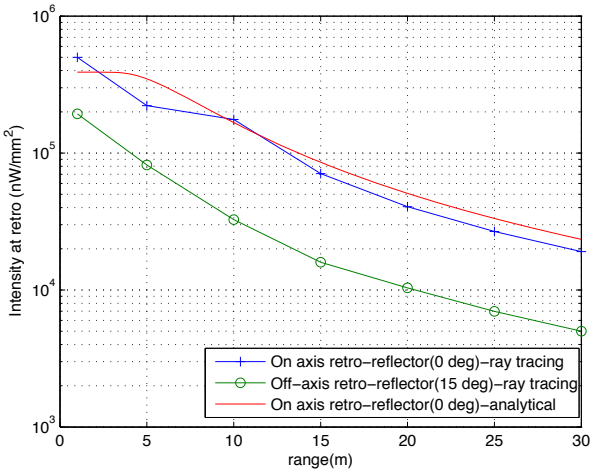

Fig. 3. Simulated illumination intensity at Smart Dust Mote

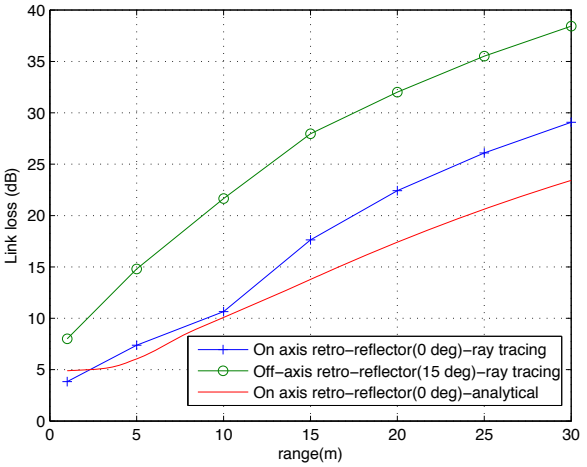

Fig. 4. Simulated link loss for on-axis and off-axis (15 degree) retro-reflectors vs. range (1mm diameter circular aperture retro-reflector)

BS after the beamsplitter) and r is the distance from BS to SDM. This assumes that the SDM is on-axis, and that the interrogating beam strikes the SDM at normal incidence (so there is no angular dependence in the equation), and that the SDM is illuminated with the peak intensity of the beam. Light passes through the aperture of the LC modulator, is retro-reflected and passes back through it once more. For a modulator with area πa_{LC}^2 (where a_{LC} is the LC modulator radius), and a retro-reflector with reflection coefficient R, the power that passes back through the aperture to be 're-emitted' and propagate back to the BS, P_{RR} can be estimated as

$$P_{RR} = I\pi a_{LC}^2 R \tag{2}$$

This light then propagates back to the BS receiver, with a divergence that is set by the diffraction from the uniformly illuminated circular aperture of the LC modulator. Assuming an airy disk diffraction pattern from the aperture the power collected at the BS receiver can be obtained by integrating this pattern over the radius of the collection lens a_{coll} to yield the received power P_R [15];

$$P_R = 0.5P_{RR}[1 - J_0^2(ka_{LC}\sin(\theta_{rec})) - J_1^2(ka_{LC}\sin(\theta_{rec}))] \tag{3}$$

where θ_{rec} is the angle subtended by the receiver at the retroreflector, and $\tan(\theta_{rec}) = \frac{a_{coll}}{r}$ where a_{coll} is the radius of the collection lens and r is the range. k is the wavenumber of the source and J_0 and J_1 are Bessel functions. The additional factor of 0.5 is included to take account of the 50/50 beamsplitter used to separate transmitted and returned beams (as shown in Figure 2(a)).

Figure 3 shows the estimated intensity at the Smart Dust Mote with range and Figure 4 shows the link loss from the aperture of the BS to the CMOS camera. This calculation estimates the link loss and intensity for what is the best case possible, where the LC modulator, retroreflector, beamsplitter and receiving optics do not introduce any loss beyond the 'ideal case' and the interrogating beam strikes the SDM at normal incidence. It also assumes diffraction limited spots illuminating the retro-reflector, and a diffraction limited return beam divergence, but for any practical system aberrations caused by the simple beam angle magnification optics will affect the illuminating spot size relative to the retro-reflector, and the divergence of the returned beam. A commercial non-sequential ray tracing programme (ZEMAX) was therefore used to model the complete optical system, as shown in Figure 2, and this was used to estimate the illumination intensity at the SDM, and the link loss. These are also shown in Figure 3 and Figure 4 for on- and off- axis (at 15 degrees off axis) retro-reflectors, indicating good agreement between analytical and ray-tracing methods for the on-axis case. The larger, more aberrated beams from the BS lead to the lower illumination intensity and higher losses off-axis.

Ray tracing shows that an intensity of approximately 5 $\mu\mathrm{W/mm}^2$ is available at a range of 30m. Measurements of the SDM (reported in more detail in section V) show that approximately 3.5 $\mu\mathrm{W/mm}^2$ is required to power the system and for the SDM receiver to operate correctly, indicating that the available illumination is sufficient to operate at a range of up to 30m. The camera has a sensitivity of 9.11 $\mu\mathrm{J/m}^2/\mathrm{DN}$ [16] where DN is a 1 bit change (at 670nm). The RMS random noise of the camera is specified as <0.5DN, and assuming a Gaussian noise distribution an approximately 3DN change is required for the camera to operate with BER of 10-9 when considering this random noise. The size of the spot of received optical power on the camera pixel array is set by the focusing lens and aberrations in the return beam, and is difficult to estimate. However, assuming a conservative value of 1mm^2 for the area of the spot, a 100 $\mathrm{bit/s}$ data rate and a requirement for a 3DN change a sensitivity of approx. -90dBm can be estimated (for a BER of 10^{-9}). If 0.39 mW is launched from the BS this leads to an available link margin of 86dB, and as the estimated link loss is 37dB for a 30m link there is approximately 50dB available for losses in the liquid crystal and other optical components. Calculations and simulations therefore indicate that the system should operate up to a range of at least 30m.

C. System Operation

1) Acquisition and tracking: During acquisition, the base station uses the camera to find the locations of the retro

TABLE I
PARAMETERS FOR SYSTEM MODELLING AND SIMULATION

BS Transmitter	
Transmitted power (at output aperture of BS)	0.39 mW (limited by eye safety)
Design wavelength	670nm
System Field of View (half angle)	15 deg
Interrogating beam half-angle (set by SLM aperture)	0.0036 deg
Retro-reflecting transceiver(RRT) Design Data rate	100 bit/s
LC Modulator radius	1 mm
Retro-reflector reflectivity (theoretical boresight maximum value) R	0.67
BS imaging receiver	
Collection lens radius	0.8 cm
Detector	1024x1024 pixel 12 bit CMOS camera
Sensitivity [16] where DN is a 1 bit change-3DN required for a BER of 10^{-9}	9.11 $\mu J/m-2/DN$ -corresponds to -60dBm for 100bit/s data stream

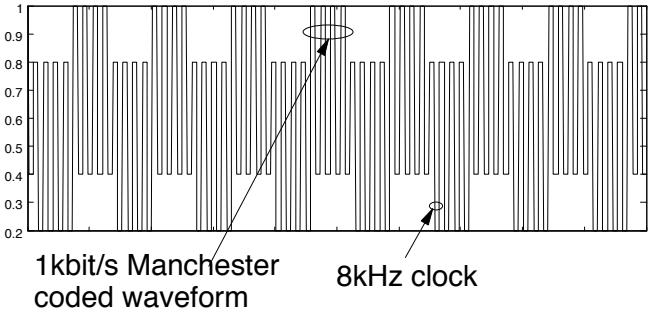

Fig. 5. Normalised intensity of the Downlink beam

reflectors by setting the camera to maximise its sensitivity and using a long exposure time. A hologram that diffuses the narrow beam across the field of view of the camera is used, and a frame is captured. (In practice 12 diffused holograms cover the entire field of view, each covering a smaller area.) A frame containing background illumination only is then subtracted from this to reduce the effect of ambient light. A filter consisting of morphological close-open pair[17] is also used to subtract the remaining background from the frame. A threshold is applied to obtain areas of high probability for an existence of a retro-reflector, which is then segmented into a connected Region of Interest (ROI). The steering phase involves converting the ROI location from the camera's axis to its steering axis. This is achieved by pre-calibrating the base station with a known target, and calculating a perspective transformation matrix between the two. The new target location is then used to steer a beam, which is then further refined by using a barrel distortion correction routine and gradient search algorithm. At this point, the base station is ready to communicate with the remote sensor. The hologram used to steer the optical beam is then switched to a DC balanced version suitable for communication [13].

2) Downlink: Figure 5 shows a schematic of the normalised intensity of the downlink beam. The consists of a 1kbit/s Manchester data waveform and an 8KHz square wave superimposed on it. Manchester encoding is used as it is well suited to the AC coupling of the receiver, having low spectral energy near DC. The square wave provides an operating clock for the SDM, because the variable operating voltage of the optically powered mote makes it very challenging to generate a fixed frequency clock.

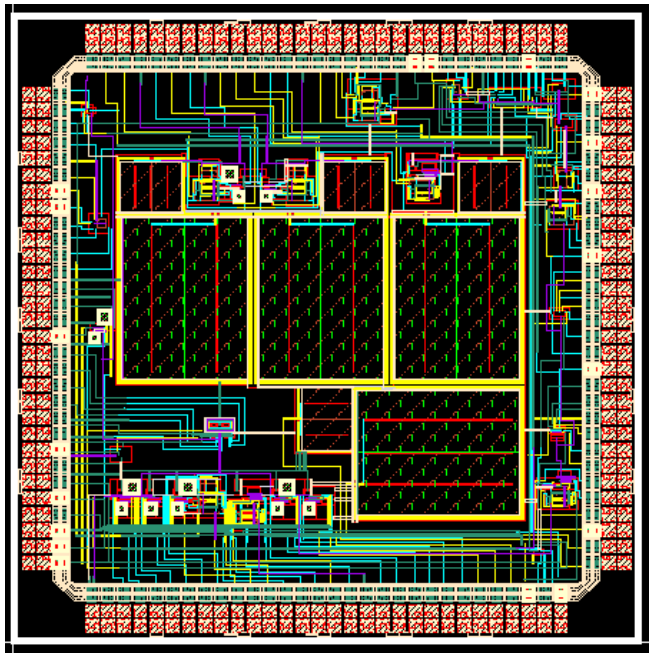

Fig. 6. Layout of smart dust integrated circuit. The large areas in the centre are different types of power photodiode. The IC is 5x5mm in size.

3) Uplink: The uplink operates by modulating the returned beam from the SDM at a low data rate (32 bit/s) using an LC cell. The bit rate was determined experimentally by measuring the LC cells available at representative operating voltages (typically 0.5-0.8V). To maximise the sampling rate of incoming modulated retro-reflected beam, the camera is set to data capture mode with a frame rate of 250 frames per second and low exposure time. Each sampling point consists of a spatially averaged intensity from pixels within the ROI determined in the acquisition phase. Once a predetermined number of samples are captured, the digitised waveform can then be filtered to reject DC wander from ambient light and out of band frequencies. The incoming Manchester code is finally processed through a Manchester decoder to recover the encoded data.

4) Network Operation: At present the BS is designed to successively interrogate SDMs, whose position is known from the initial tracking phase. The BS will steer the downlink to the appropriate position, 'wake' the SDM by illuminating it, and then command it to perform a task and report results on the MRR. However, the flexibility of the hologram allows it to route light to different SDMs, and the parallel nature of the camera receiver will allow multiple data streams to be recovered. It should therefore be possible to use a shared downlink and individual uplink architectures if this is appropriate.

IV. SMART DUST MOTE

Figure 1 also shows a schematic of the SDM considered here, and Figure 6 shows a layout of one of the integrated circuits fabricated in the project. The SDM consists of a power photodiode, a communications receiver and associated

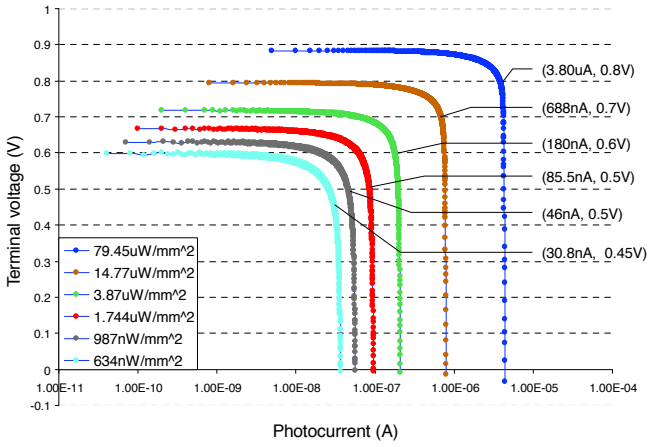

Fig. 7. The measured load lines of a pair of photodiodes connected in series at different optical power densities (measured at 830nm)

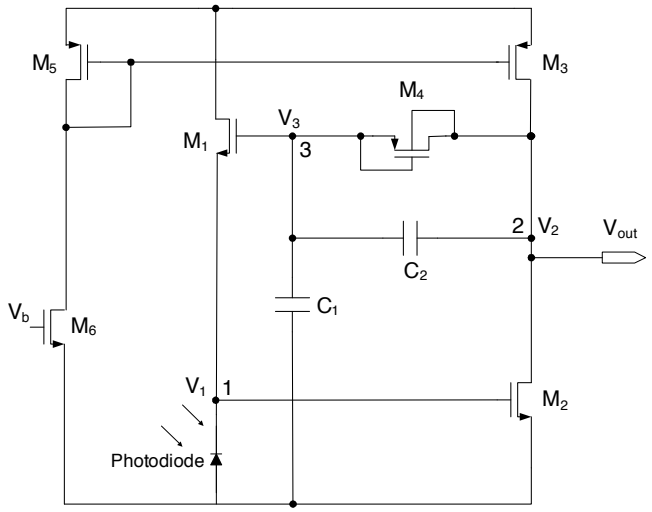

Fig. 8. The adaptive photodetector circuit used in the smart dust mote

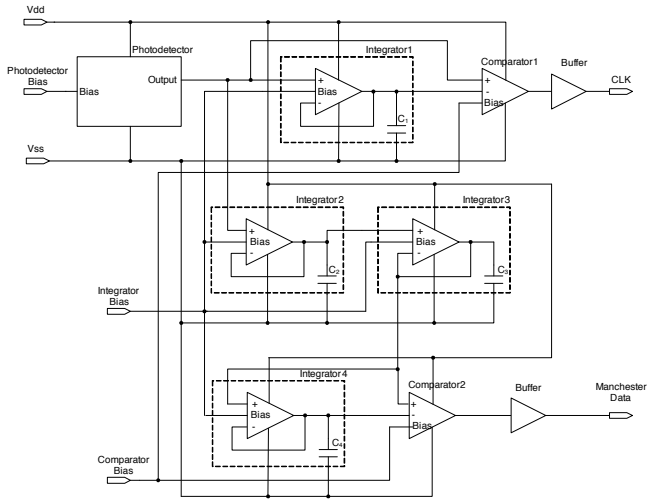

Fig. 9. A diagram of the system that is used to separate the two digital signals modulated onto the downlink beam. The downlink is used to send ASCII codes for 'u' (up) and 'd'(down) which are used to switch the state of the LC modulator. An instruction decoder is used to interpret the ASCII codes and generate a signal to drive the LC modulator, which is described in the next section.

circuitry (all implemented in the IC), and a modulated retro-reflector. Each of these is described in more detail below.

A. Providing power

Two series connected photodiodes are used to provide power to the SDM. In order to allow series connection of diodes a triple well UMC $0.18\mu\mathrm{m}$ 1P6M Mixed-mode process is used. With this process it is possible to use the Nwell and Psub layers of this process to create one diode that can be connected in series with another photodiode created using the Pwell and Twell layers of the process. These combinations of layers create diodes that are at different depths below the surface of the silicon and have different depletion widths. To compensate for the resulting lower quantum efficiency of the shallower junction diode the area of this diode needs to be larger than the other diode. In the substrates that have been manufactured the Nwell/Psub photodiode had an area of $0.2\mathrm{mm}^2$ whilst the area of the Pwell/Twell photodiode is $1.3\mathrm{mm}^2$. Figure 7 shows the load lines of two series connected diodes illuminated with different intensities at 830nm. These show that a supply voltage of 0.6-0.9V is available for load currents of between 10-1000nA, depending on the intensity of the illumination. Any SDM circuitry must operate within these limits.

B. Communications receiver

The receiver must be able to operate at the required bandwidth, with a wide dynamic range. For the data rates considered here the use of CMOS camera pixel designs is attractive. Pixels with a logarithmic response can be designed to respond to the contrast ratio of the modulation, rather than the absolute received power, offering wide dynamic range without the need for limiting post-amplification. Figure 8 shows the design of an adaptive receiver with these characteristics, which is based on a design reported in [18]. This operates successfully for mean photocurrents of between 100pA and 100nA. As described earlier the downlink waveform consists of a $1\mathrm{kbit/s}$ Manchester data stream combined with an 8kHz clock. Figure 9 shows circuitry that both recovers the Manchester waveform, and the 8kHz clock. The clock is then divided down and used in circuitry to recover and retime the binary data from the received Manchester data.

C. Modulated Retro-reflector

1) LC cells: For the reasons stated above LC cells were chosen to form the modulator. It is challenging to design cells that will provide significant optical modulation with the operating voltages available, and for this reason stacked diodes were incorporated into IC designs, in order to provide 0.7V to switch the devices. Nematic cells approximately $3\mu\mathrm{m}$ thick, using anti-parallel alignment with SiOx alignment layers, were fabricated to provide the modulators. Ionic and non-ionic LC materials were investigated. In both cases the LC responds to the magnitude of the electric field, but in the ionic case there is a requirement to have zero net electric field on the LC over time. Different LCs therefore require different drive circuits, and a number of different options were investigated. For the results reported here an ionic LC cell filled with standard nematic liquid crystal E7 is used. These devices have a capacitance of $28\ \mathrm{pF/mm}^2$ so for drive voltages of 0.5V the switching energy is approximately $7\ \mathrm{pJ/bit/mm}^2$.

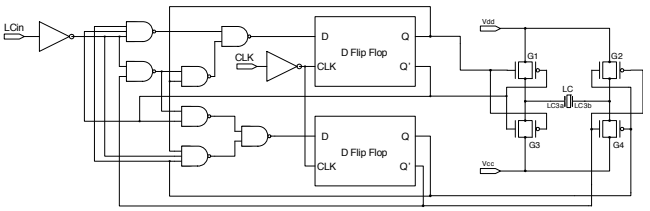

Fig. 10. A schematic diagram of the logic circuits and pass gates used to modulate the voltage on the liquid crystal cell.

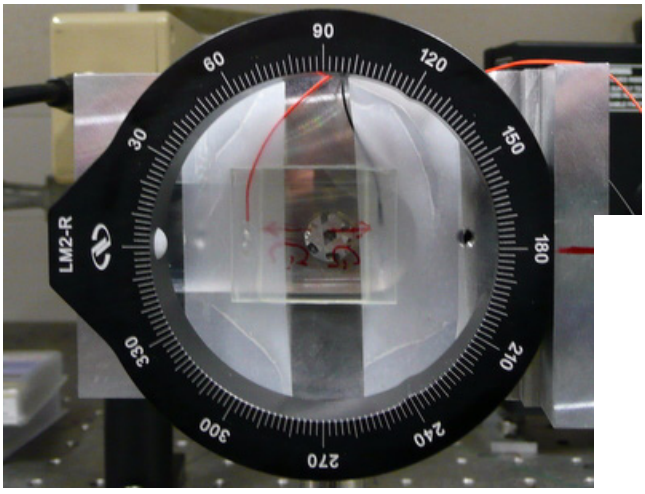

Fig. 11. Modulated retro-reflector

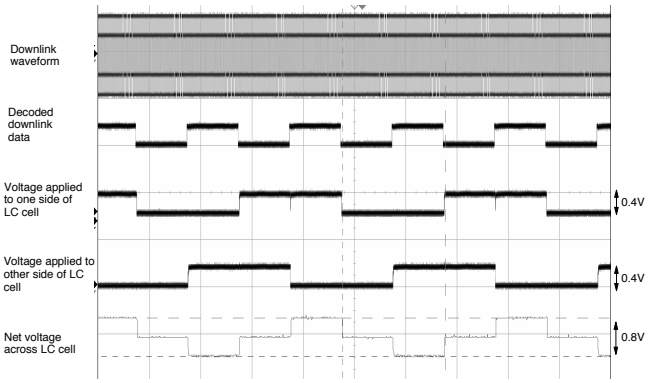

Fig. 12. The measured response of a optically powered mote. The modulation of the downlink beam is shown at the top of the figure. Also shown are the resulting input to the liquid crystal modulator circuit, the voltages that would be applied to each side of the liquid crystal cell and the differential voltage

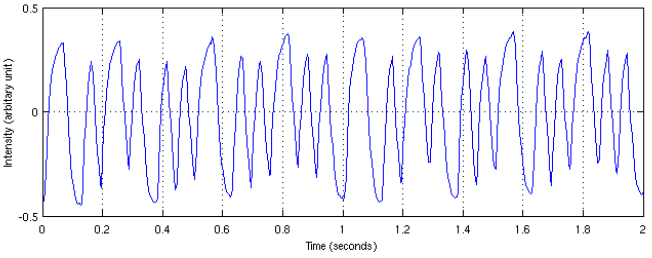

Fig. 13. Received waveforms from retro-reflecting uplink

2) LC drive circuitry: Figure 10 shows a diagram c circuitry used to drive the ionic LC. This can apply +Vd 0, -Vdiode across the LC, thus allowing DC balanci apply where Vdiode is the voltage from a two series conr diodes

3) Retro-reflectors: High-quality compact retro-refl structures are challenging to manufacture. In this case a mercially available moulded part [19]was modified to cr retro-reflector approximately 1.5mm in diameter. A polariser is placed in front of the LC cell which is placed in front of the retro-reflector. Figure 11 shows the LC cell mounted in front of the retro-reflector. (This is in an experimental non-integrated form.)

V. System Results

A. Downlink and SDM operation

The SDM was illuminated with a downlink waveform containing 'u' and 'd' codes, and an average intensity of 3.5 $\mu W/mm^2$. A 1nF external storage capacitor is connected across the power rails to provide a store of charge, and a 100pF capacitor connected in place of the LC modulator in order to simulate its effect. The SDM contained bias generating circuits that did not operate as predicted due to process calibration issues so several biases in the circuit are externally generated. (A further iteration of the IC design cycle would allow this to be resolved). Figure 12 shows the response of the SDM. This shows the SDM operating correctly, and that the successive 'u' and 'd' signals are translated to the operating voltages required for the LC cell. In this case switching energies are approximately 16pJ/bit switched for the 100pF capacitor (as the voltage supplied to the modulator is approximately 0.4V in this case). The estimated electrical power consumption is approximately 100nA at 0.4V or 40nW.

B. Base station tracking

Tracking error was reduced by using an estimate of the barrel distortion of the optical system determined using ray-tracing, and making a pre-correction to the steering angles required to direct light to a particular SDM based using this estimate. In order to measure the performance of the correction a rectangular calibration board consisting of 90 equally spaced retro-reflectors was used to provide targets for error measurements. In addition, there were three retro-reflectors surrounding the board to test tracking performance at larger divergence. Each target was acquired and tracked, and a gradient search algorithm was used to find maximum return intensity (which was considered to be the desired steering direction). The mean tracking error (the correction applied by the gradient search) was reduced from 53 to 47 μrad, a reduction of 11%.

C. Uplink operation

An MRR of the type shown in Figure 11 was used to transmit data to the BS. Figure 13 shows a waveform of a 32 bit/s Manchester coded waveform received by the base station at a distance of 15 m under low ambient light conditions and a sampling (frame) rate of 250 $samples/s$. In order to assess the effect of operating voltage and ambient noise the link was

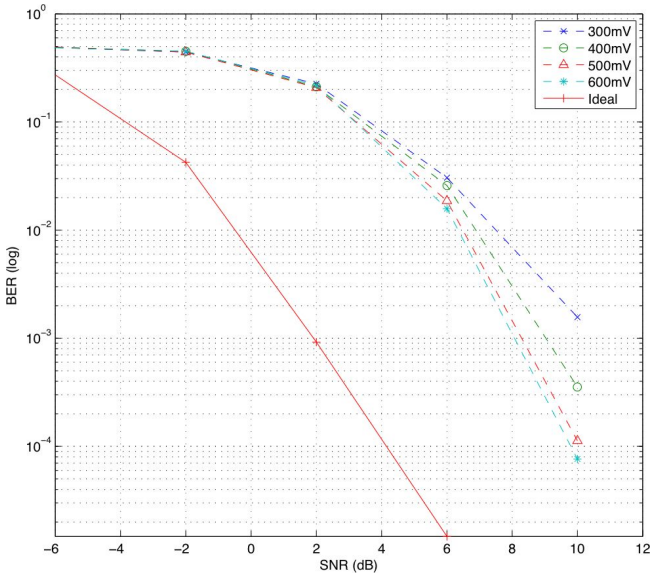

Fig. 14. Estimated BER for a nominal LC cell operating voltage of 500mV

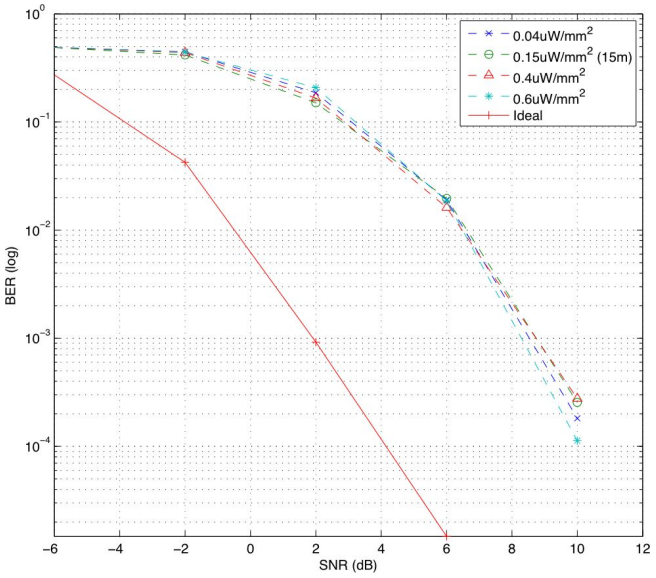

Fig. 15. Plot of BER vs. SNR for different beam power densities

operated in a dark room with different LC voltages at a range of 3m. The received waveforms that are recorded are degraded by Inter-symbol Interference (ISI) introduced by the low LC switching speed, but are not effected by noise, due to the low light conditions and high received signal. The additional effect of noise was then simulated by adding Additive White Gaussian Noise (AWGN) to these 'clean' waveforms so the combined effect of camera noise[20], ambient light noise[21] and operating voltage could be estimated. Data recovery was achieved by using a bandpass filter with a passband from 1.56Hz - 32Hz followed by a matched filter to maximise performance[22]. The Manchester data rate was fixed to $32\mathrm{bit/s}$, with 10^7 bits tested for each data point. Figure 14 shows the BER plot for varying liquid crystal drive voltages, with nominal operating voltage of 500mV. As a reference, the BER performance of the system using an ideal waveform is also plotted. It can be seen that higher drive voltage results in lower BER, up to the nominal voltage of 500mV. A plot of BER versus signal to noise ratio (SNR) of varying beam power densities is show in Figure 15. The nominal operating density is $0.6\mu\mathrm{W/mm^2}$ and the drive voltage used for the liquid crystal shutter is fixed to 500mV. Note that these densities are lower than required to power the sensor, and indicate that the range is limited by the need to illuminate and power the SDM, rather than correct operation of the retro-reflecting uplink. At present the SDM and the uplink have been separately tested, and both show correct operation. System integration is currently underway, and there are several unresolved challenges: the system was originally designed to operate at 830nm and the SDM measurements are made at this wavelength. The alignment of the BS components and testing of the tracking algorithms is more straightforward in the visible, so the BS currently operates at 670nm. As the performance of the photodiodes is better at 670nm than 830nm the SDM measurements represent a conservative limit of lower intensity. The final aim is operate the system at 785nm, as measurements indicate this is the best available non-visible wavelength at which to operate. The other challenge is the geometry of the system and the required illumination spot size. The diodes on the SDM occupy a footprint of approximately 1.5x1.5mm and the retro-reflector is presently 1x1mm across, so the total area to be illuminated might be $< 4\ \mathrm{mm^2}$. However, close integration of these is challenging, so a single spot of $1\mathrm{cm^2}$ might be required for the hybrid currently being constructed. The available power from the base station is not presently sufficient to create the $3\mu\mathrm{W/mm^2}$ required (as the power emitted from the BS is limited to $30\mu\mathrm{W}$ rather than the 0.5mW required). This should be solved by both closer integration and the use of a higher laser power.

VI. Conclusions

Communicating with, and powering small silicon based systems will become increasingly challenging and optical wireless techniques are attractive in that they can easily combine both these functions. In this paper we demonstrate that it is possible to communicate over 10s of metres with systems that can also be powered by the interrogating beam. Low communications energies of $16\mathrm{pJ/bit/mm^2}$ of modulator are achieved, and it should be possible to reduce these further. The total electrical power consumption of the mote is approximately 40nW. The next stage of this work is to integrate the communications modulator and the silicon IC to create a compact dust mote, and to test the system at the final design wavelength. In the longer term work will focus on increasing the functionality of the system, in terms of both processing power, and the ability to make measurements and sense the environment around it.

References

[1] Specknet collaboration, www.specknet.org, Accessed Jan 2009.
[2] J. M. Kahn, R. H. Katz, and K. S. Pister, *Next century challenges: mobile networking for "Smart Dust"*' 1999.
[3] B. Warneke, M. Last, B. Liebowitz, and K. S. J. Pister, *Smart Dust: communicating with a cubic-millimeter computer*, Computer, vol. 34, pp. 44-51, Jan. 2001.

[4] K. S. J. Pister, *Smart dust-hardware limits to wireless sensor networks*, in 23rd International Conference in Distributed Computer Systems ICDCS 2003. 19 22 May 2003 Providence, RI, USA, 2002, p. xviii+697.
[5] K. Romer, *Tracking real-world phenomena with smart dust*, in Wireless Sensor Networks. First European Workshop, EWSN 2004. Proceedings. 19 21 Jan. 2004 Berlin, Germany, 2004, p. xiv+363.
[6] D. C. O'Brien, W. W. Yuan, J. J. Liu, G. E. Faulkner, S. J. Elston, S. Collins, and L. A. Parry-Jones, *Optical wireless communications for micromachines*, in Free-Space Laser Communications VI, 2006, p. 63041A.
[7] Semiconductor Industry Association.www.sia-online.org, Accessed May 2009.
[8] Lixia-Zhou, J. M. Kahn, and K. S. J. Pister, *Corner-cube retroreflectors based on structure-assisted assembly for free-space optical communication*, J. Microelectromechanical Systems, vol. 12, pp. 233-42, June 2003.
[9] G. Gilbreath, W. S. Rabinovich, T. J. Meehan, M. J. Vilcheck, R. Mahon, R. Burris, M. Ferraro, I. Sokolsky, J. A. Vasquez, C. S. Bovais, K. Cochrell, K. C. Goins, R. Barbehenn, D. Katzer, K. Ikossi-Anastasiou, and M. J. Montes, *Compact lightweight payload for covert data link using a multiple quantum well modulating retro-reflector on a small rotary-wing unmanned airborne vehicle*, 2000, pp. 57-67.
[10] Z. Lixia, K. S. J. Pister, and J. M. Kahn, *Assembled corner-cube retroreflector quadruplet Technical Digest*, Robotics & Autom, 2002.
[11] A. V. Krishnamoorthy and D. A. B. Miller, *Scaling optoelectronic-VLSI circuits into the 21st century: a technology roadmap*, 1996.
[12] D. C. O'Brien, R. J. Mears, T. D. Wilkinson, and W. A. Crossland, *Dynamic holographic interconnects that use ferroelectric liquid-crystal spatial light modulators*, Applied Optics, vol. 33, pp. 2795-803, 10 May 1994.
[13] P. Vachiramon, G. E. Faulkner, and D. C. O'Brien, *A DC balancing algorithm for FLCOS binary phase holograms*, Optics Letters, vol. 32, pp. 3275-7, 15 Nov. 2007.
[14] W. S. Rabinovich, P. G. Goetz, R. Mahon, L. Swingen, J. Murphy, M. Ferraro, J. H. R. Burris, C. I. Moore, M. Suite, G. C. Gilbreath, S. Binari, and D. Klotzkin, *45-Mbit/s cat's-eye modulating retroreflectors*, Optical Engineering, vol. 46, pp. 104001-8, 2007.
[15] M. Born and E. Wolf, Principles of Optics: Electromagnetic Theory of Propagation, Interference and Diffraction of Light. Cambridge: Cambridge University Press, 1999.
[16] Photon Focus, Photon Focus MV-1024 Camera.
[17] R. C. Gonzalez, R. E. Woods, and S. L. Eddins, *Digital Image processing using MATLAB*, Upper Saddle River, N. J.: Pearson Prentice Hall, 2004.
[18] T. Delbrück and C. A. Mead, *Analog VLSI phototransduction by continuous-time, adaptive, logarithmic photoreceptor circuits, Vision Chips: Implementing vision algorithms with analog VLSI circuits*, in Vision Chips: Implementing vision algorithms with analog VLSI circuits, C. Koch and H. Li, Eds.: IEEE Computer Society Press, 1995, pp. 139-161.
[19] Edmund Optics, Corner cube array NT47-321.
[20] T. Hui, B. Fowler, and A. E. Gamal, *Analysis of temporal noise in CMOS photodiode active pixel sensor*, IEEE J. Solid-State Circuits, vol. 36, pp. 92-101, 2001.
[21] K. Samaras, A. M. Street, D. C. O'Brien, and D. J. Edwards, *BER performance of various line coding schemes in the presence of Gaussian noise and intersymbol interference*, in 4th Communications Networks Symposium, Manchester, 1997.
[22] F. Guilloud, E. Boutillon, and J. L. Danger, *Bit error rate calculation for a multiband non-coherent on-off keying demodulation*, in Communications, 2002. ICC 2002. IEEE International Conference on, 2002, pp. 202-206.

Dominic O'Brien Dominic O'Brien is a Reader in Engineering Science at the University of Oxford, and leads the optical wireless communications group. He gained MA(1991) and PhD (1993) Degrees from the Department of Engineering at the University of Cambridge. From 1993-1995 he was a NATO fellow at the Optoelectronic Computing Systems Center at the University of Colorado. His current research is in the field of optical wireless systems. He is the author or co-author of approximately 130 publications or patents in the area of optics and optoelectronics.

Jing Jing Liu Jing Jing Liu received his BEng with 1st class honours (2003) and MEng (2005) in electronics engineering from Nanyang Technological University, Singapore. After working as an IC design engineer in International Rectifier Southeast Asia for half a year, he pursued his D.Phil degree in Department of Engineering Science at University of Oxford. Currently, he is doing a postdoctoral work in Oxford and his research interests include CMOS weak inversion design and RFIC design.

Grahame E. Faulkner Mr Grahame Faulkner is a Research Assistant in the Department of Engineering Science. He received his B.Sc. honours in physics and microelectronics from Oxford Brookes University. He has over 10 years of experience in the field of optical wireless communications, optical interconnects and optoelectronic integration.

Vachiramon Pithamiron Mr Pithawat Vachiramon received his MEng degree from University of Oxford and currently working towards a DPhil in free-space optical wireless communications. His areas of interest includes wireless communications, computer generated holography and turbulence mitigation.

Sashigaran Sivathasan Dr Sashigaran Sivathasan is a Senior Lecturer at Curtin University of Technology (Malaysian campus). He gained his MSc degree in Communications and Signal Processing from the Imperial College, University of London in 2001. He received his DPhil degree from the University of Oxford in 2008. His current research is in the field of wireless sensor networks.

Wei Wen Yuan Biography not available

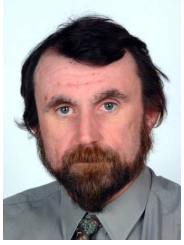

Steve Collins Steve Collins received the B.Sc. degree in theoretical physics from the University of York, York U.K. in 1982 and the Ph.D degree from the the University of Warwick, Warwick, U.K. in 1986. From 1985 until 1997, he worked within the Defence Research Agency on various topics including the origins of 1/f noise in MOSFETs, imaging sensors and analog information processing. Since 1997 he has been with the University of Oxford, Oxford, U.K. where he has continued his interest in CMOS imaging sensors.

Steve J. Elston Biography not available